Journal of ELECTRONIC MATERIALS, Vol. 49, No. 7, 2020
https://doi.org/10.1007/s11664-020-08174-y

Structural, Piezoelectric and Dielectric Properties of $K_{0.4}Na_{0.6}NbO_3$-$Bi_{0.5}Li_{0.5}ZrO_3$-$CaZrO_3$ Ternary Lead-Free Piezoelectric Ceramics

CAIWANG HE,[1] XUDONG BAI,[1] JINCHUAN WANG,[1] YUNYI LIU,[1] YANG LU,[1] XIAOKUI LIU,[1] YUNJIE XIANG,[1] ZUNPING XU,[1] and YI CHEN [1,2,3]

1.—School of Materials and Energy, Southwest University, Chongqing 400715, People's Republic of China. 2.—National and Local Joint Engineering Laboratory of Intelligent Transmission and Control Technology (Chongqing), Southwest University, Chongqing 400715, People's Republic of China. 3.—e-mail: mrchenyi@swu.edu.cn

The $Bi_{0.5}Li_{0.5}ZrO_3$ and $CaZrO_3$ co-modified (K,Na)NbO_3-based ceramics, with a formula of $(0.98\text{-}x)K_{0.4}Na_{0.6}NbO_3$-$xBi_{0.5}Li_{0.5}ZrO_3$-$0.02CaZrO_3$, were designed to form a rhombohedral-tetragonal phase boundary, and a conventional solid-state sintering method was employed to prepare them. X-ray diffraction analysis revealed that a pure perovskite structure could be maintained in the studied composition range $0 \le x \le 0.05$. Dielectric-temperature measurements were performed to further identify the phase structure of the ceramics, which was found undergoing a gradual evolution from an orthorhombic to a rhombohedral structure with increasing x. Furthermore, a rhombohedral-tetragonal phase boundary was observed to be formed at $x = 0.035$, near which enhanced piezoelectric properties were obtained, with piezoelectric constant $d_{33} = 241$ pC/N and planar electromechanical coupling coefficient $k_p = 0.37$. Additionally, an investigation was conducted of the influence of $Bi_{0.5}Li_{0.5}ZrO_3$ addition on the microstructure and paraelectric-ferroelectric phase transition of the ceramics as well. We believe that the findings in this current work can deepen our understanding of the role of $Bi_{0.5}Li_{0.5}ZrO_3$ in the construction of a phase boundary and improvement of piezoelectric properties for (K,Na)NbO_3-based ceramics.

Key words: Lead-free ceramics, piezoelectric properties, dielectric properties, niobates, phase boundaries

INTRODUCTION

$Pb(Zr,Ti)O_3$ (PZT)-based ceramics are still the most extensively applied piezoelectric materials in many electronic devices.[1,2] However, lead, which accounts for over 68 wt.% of the total content in PZT-based ceramics, will soon be restricted from use in electronic products by many countries and regional organizations,[1,2] due to its serious harm to the environment. Therefore, the need to develop lead-free alternatives to PZT-based piezoelectric materials is urgent. (K,Na)NbO_3 (KNN)-based ceramics, which have good piezoelectric properties and a relatively high Curie temperature (T_C),[1–3] are among the most promising lead-free candidate materials to replace PZT for practical application. Nevertheless, there is a large gap in piezoelectric activity between pure KNN and commercial PZT-based ceramics.[4]

(Received November 26, 2019; accepted April 29, 2020; published online May 7, 2020)

A valid way to improve the piezoelectric activity of KNN-based ceramics is through partial substitution of them with other cations or ABO_3-type compounds,[1,5,6] especially those that can form a phase boundary.[5,6] As is well known, phase boundaries can yield a high alignment of ferroelectric dipoles during poling, owing to the creation of more spontaneous polarization directions,[1] and enhanced piezoelectric activity may thus be generated for ceramics with a phase boundary. There are two phase transitions below T_C for pure KNN, including a rhombohedral–orthorhombic (R–O) phase transition occurring at −123°C and an orthorhombic–tetragonal (O–T) phase transition at 210°C.[7] Many additives can shift the temperature of the R–O or O–T phase transition (T_{R-O} or T_{O-T}) of KNN to room temperature, thereby resulting in the construction of an R–O or O–T phase boundary.[8,9] Unfortunately, the piezoelectric properties for KNN-based ceramics with an R–O or O–T phase boundary are still inferior to those of commercial PZT-based materials.

Piezoelectric properties comparable to PZT were only recently achieved in KNN-based ceramics when a series of new KNN ceramic systems, possessing a rhombohedral–tetragonal (R–T) phase boundary, were successfully developed by Wu et al.[10–12] The R–T phase boundary in KNN-based ceramics, which consists of the same two phases as the morphotropic phase boundary (MPB) of PZT, is constructed by merging the T_{R-O} and T_{O-T} into a temperature[13,14] known as T_{R-T}. Dopants such as Sb^{5+} play an important role in the construction of the R–T phase boundary, as they can move both the T_{R-O} and T_{O-T} to room temperature simultaneously.[15] BMZ-type compounds (B = bismuth, M = alkali metals and Z = zirconium) are found to have a similar effect on the two temperatures, and excellent piezoelectric properties have been achieved in many BMZ-modified KNN-based ceramics.[16] Adding $CaZrO_3$ to KNN is reportedly also able to change the T_{R-O} and T_{O-T}, and additionally can improve the thermal stability of electrical properties.[17]

In this current work, we added $Bi_{0.5}Li_{0.5}ZrO_3$ and $CaZrO_3$ into KNN to form a new ternary ceramic system $(0.98 - x)K_{0.4}Na_{0.6}NbO_3$-$xBi_{0.5}Li_{0.5}ZrO_3$-$0.02CaZrO_3$ (abbreviated as KNN-xBLZ-CZ). The reason that the $Bi_{0.5}Li_{0.5}ZrO_3$ was selected to be as an additive rather than other BMZ-type compounds is due to the better roles of adding Li^+ into KNN-based ceramics in increasing the T_C and improving the sintering activity.[18,19] With reference to the results of a previous article,[20] a relatively high Na/K ratio was designed in the ceramic system, also aiming to improve the sintering activity. The effect of BLZ incorporation on the phase structure of the ceramics was investigated, and an R–T phase boundary was found to be formed at $x = 0.035$, near which the ceramics exhibited enhanced piezoelectric properties.

EXPERIMENTAL PROCEDURE

A standard solid-state sintering route was applied to prepare the KNN-xBLZ-CZ ceramics ($x = 0$, 0.02, 0.03, 0.035, 0.04 and 0.05). The starting materials consisted of K_2CO_3 (99%), Na_2CO_3 (99.8%), Nb_2O_5 (99.5%), Li_2CO_3 (98%), ZrO_2 (99%), $CaCO_3$ (99%) and Bi_2O_3 (99%) powders. These starting powders were calcined at 850°C for 6 h, following a process of mixing and milling for 24 h with ZrO_2 balls and anhydrous alcohol as the medium. These calcined powders were ground again and followed by mixing with 3–5 wt.% polyvinyl alcohol (PVA) for granulation. The granulated powders were then compacted into 10-mm-diameter disc-shaped pellets averaging 1 mm in thickness. The green bodies were placed in a muffle furnace, which was subsequently heated to 500°C and held for 2 h to remove the PVA binder. After that, the furnace was heated to a temperature ranging from 1140°C to 1180°C (depending on the sample) and maintained for 3 h, for the densification of the ceramic green pellets.

The crystal structures of the KNN-xBLZ-CZ ceramics were determined by an x-ray diffraction (XRD) method. A scanning electron microscope (SEM) was used to conduct microscopic observation. Density measurements of the sintered ceramic samples were performed using the Archimedes method. The ceramics used for electrical characterization were coated by silver paste on their two surfaces, followed by a firing step at 650°C for 10 min. A ferroelectric test system was employed to obtain their polarization–electric field (P–E) hysteresis loops, and temperature-dependent dielectric behavior was tested in the temperature range of about −100 to 150°C and room temperature to 450°C using an LCR analyzer (E4980A, Keysight Technologies, USA) combined with a temperature-controlled furnace. The electrode-coated ceramic samples used for piezoelectric characterization were polarized in a room-temperature silicone oil bath under a DC field of 3–4 kV/mm for 30 min. After aging in air for over 24 h, the piezoelectric constants d_{33} of the polarized ceramics were determined on a quasi-static d_{33} meter, and their planar electromechanical coupling coefficient k_p was measured by an impedance meter based on the resonance/anti-resonance method.

RESULTS AND DISCUSSION

Figure 1a shows the XRD images of KNN-xBLZ-CZ ceramics, measured between $2\theta = 20°$ and 60°. All the XRD peaks could be assigned to a perovskite structure and no other XRD peaks were detected,

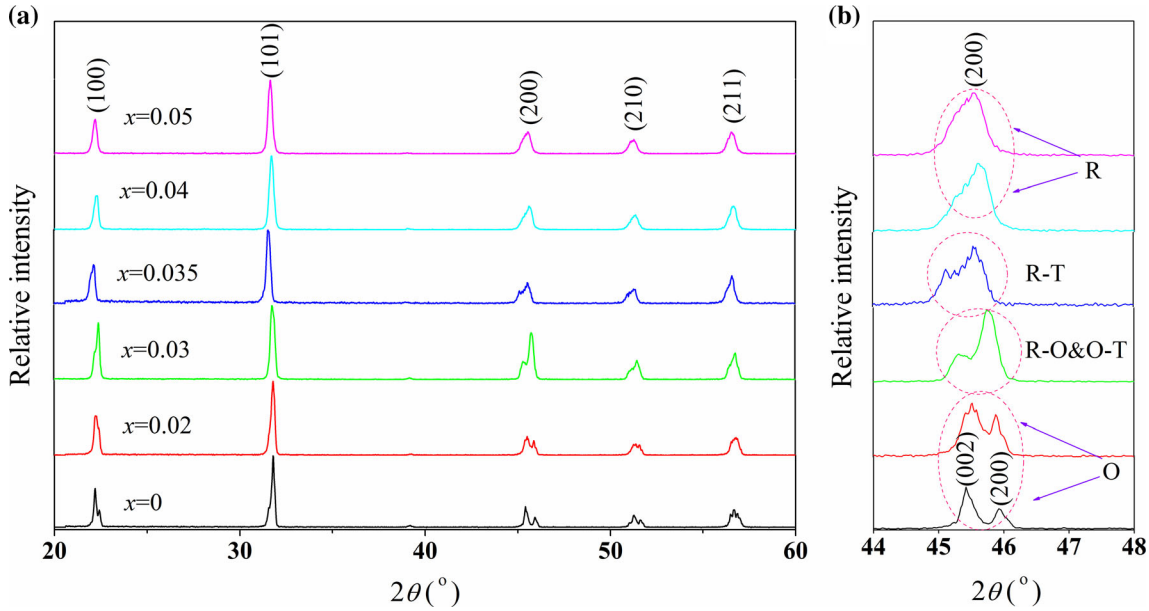

Fig. 1. XRD images of KNN-*x*BLZ-CZ ceramics in the 2θ range of (a) 20°–60° and (b) 44°–48°.

implying the formation of stable solid solutions throughout the studied composition range. For better identification of the structure evolution, the enlarged views of the XRD images between 44° and 48° are exhibited in Fig. 1b. It is clearly found from Fig. 1b that there are two sub-peaks at around 45° for the ceramics with a relatively low BLZ addition content, which can be indexed as (002) and (200) planes of perovskite structure, respectively. The relative intensity of the (002) sub-peak is clearly higher than that of the (200) sub-peak for x = 0–0.02, indicating that these compositions should have an orthorhombic structure.[21] However, with x increased to 0.03–0.035, the (200) sub-peak shows a higher relative intensity, which suggests that there should have a phase transition near here. With a further increase in BLZ content, the two sub-peaks merged into a single XRD peak, signifying that the ceramics with $x \geq 0.04$ possess a rhombohedral symmetry, as suggested by many previous articles.[3,5,22]

For more detailed identification of the structure evolution of KNN-*x*BLZ-CZ ceramics, especially for those with compositions near x = 0.03–0.035, the temperature-dependent dielectric constants (ε_r) of the ceramics were measured from around −100°C to 150°C, as shown in Fig. 2. There are clearly two anomalies on the curves for the ceramics with x = 0.02, which correspond to T_{R-O} and T_{O-T}, respectively. However, both the T_{R-O} and T_{O-T} are slightly far from room temperature, suggesting that the composition x = 0.02 has an orthorhombic structure, in accord with the previous inference based on XRD analysis. The T_{R-O} and T_{O-T} are then moved to near room temperature with x = 0.03, implying that there should be coexistent R–O and O–T phase transitions near here. The two dielectric anomalies eventually merge into a single one at x = 0.035, which indicates the formation of an R–T phase boundary. When $x \geq 0.04$, no obvious dielectric anomaly can be observed on the dielectric-temperature curves, and this is because their structures have transitioned to a pure rhombohedral symmetry. All the results of structural identification are marked in Fig. 1b. To sum up, the BLZ incorporation in KNN-based ceramics is a very beneficial way for the construction of a phase boundary, as it can shift both the T_{R-O} and T_{O-T} to room temperature.

Figure 3 presents the morphologies of the KNN-*x*BLZ-CZ ceramics with different BLZ contents. While there are some pores, all the ceramic samples exhibit a relatively dense microstructure. The grains of all the compositions are mainly in the shape of a cuboid. Additionally, the compositions x = 0–0.03 show an obviously bimodal distribution in grain sizes in which the large grains coexist with many fine ones, which is a frequent phenomenon in KNN-based ceramics modified by Sb^{5+} or Zr^{4+} ions.[23,24] Finally, the grain size is noted to decrease with increasing BLZ content. For better analysis of the relationship between grain size and composition, the average grain size of each composition was determined by the linear intercept method, as

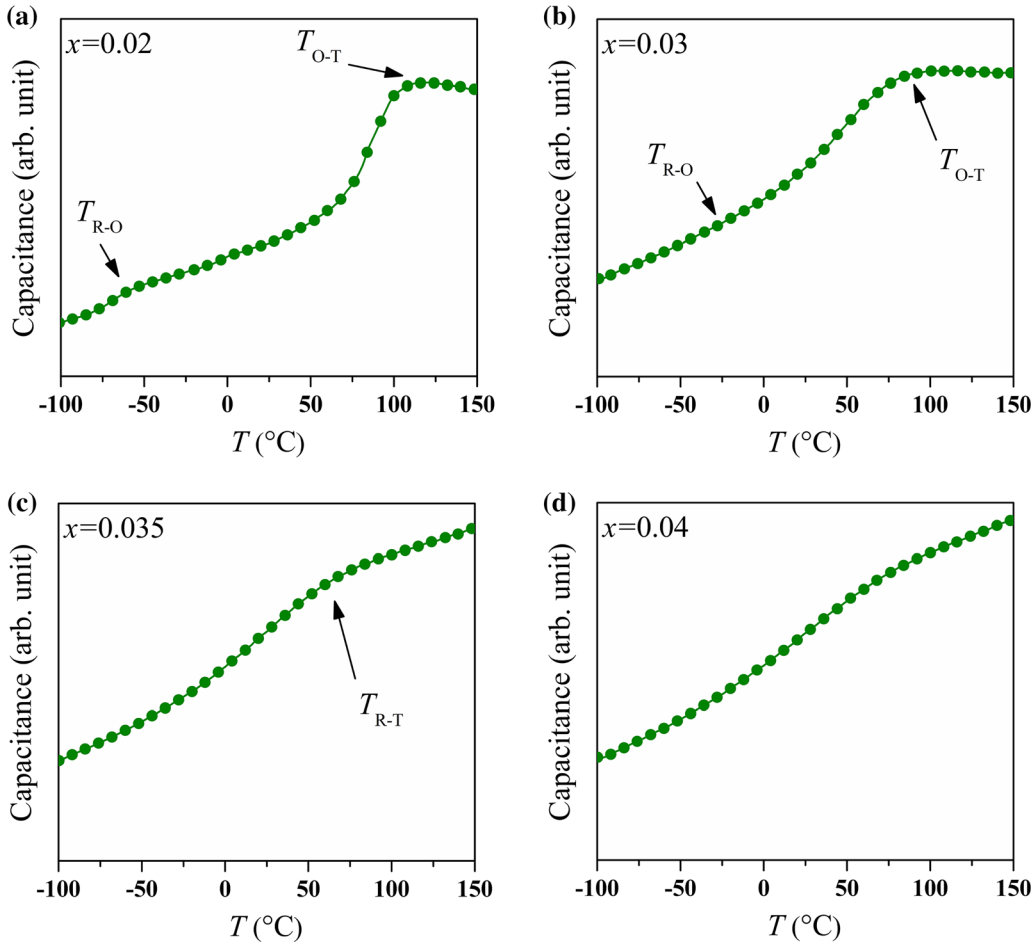

Fig. 2. Temperature-dependent dielectric constants of KNN-*x*BLZ-CZ ceramics, measured from about −100°C to 150°C with (a) $x = 0.02$, (b) $x = 0.03$, (c) $x = 0.035$ and (d) $x = 0.04$.

shown in Fig. 4. One can note that the average grain sizes are very low (< 0.6 μm) with $x \geq 0.03$, which may be attributed to the aggregation of Bi^{3+} and Zr^{4+} ions at the grain boundaries that consequently hinders the growth of grains during sintering, as suggested by previous articles.[13,25–27] When $x \geq 0.035$, the grains become so extremely fine that the phenomenon of bimodal distribution almost disappears.

The relationship between density and BLZ content of KNN-*x*BLZ-CZ ceramics is demonstrated in Fig. 5 for further evaluation of the sintering quality. The density is found to maintain an upward trend with the increase of BLZ content until $x = 0.035$, and this can be due to the greater molecular weight of BLZ than that of KNN. The trend, however, is reversed with a further increase of x. It is the lowered sintering activity, which is caused by the aggregation of Bi^{3+} and Zr^{4+} ions at the grain boundaries (as discussed previously), that leads to the reversed variation in density.

The temperature-dependent dielectric constants of KNN-*x*BLZ-CZ ceramics were also measured from room temperature to 450°C to investigate the characteristics of their paraelectric-ferroelectric phase transitions, as illustrated in Fig. 6. It is found that there exists a clear peak on the dielectric-temperature curves for the ceramics with a relatively low BLZ content. The temperature of the dielectric peak is frequently determined as the Curie temperature (T_C). The Curie peak tends to widen with increasing BLZ content, displaying the onset of diffuse phase transition. The diffuseness of phase transition is generally considered to be associated with chemically inhomogeneous micro-regions in KNN-based solid solutions,[28] and obviously it is the BLZ incorporation into the matrix that induces the composition inhomogeneity of micro-regions in this work. Additionally, the T_C is noted to tend to decline with increasing BLZ content, just like the effect of adding other BMZ-type compounds to KNN on it.[10,16,29] Nevertheless,

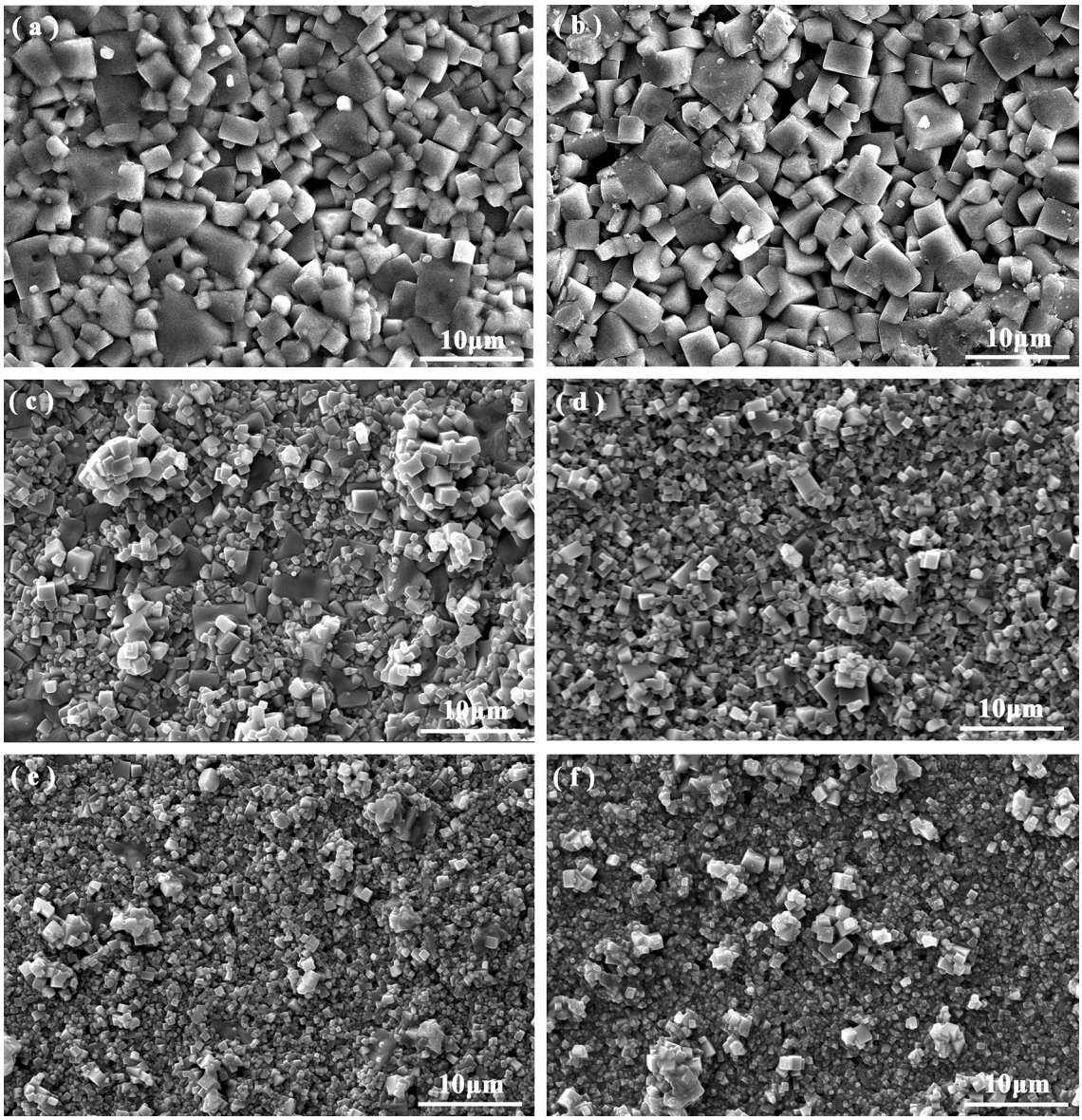

Fig. 3. SEM surface micrographs of KNN-*x*BLZ-CZ ceramics with (a) $x = 0$, (b) $x = 0.02$, (c) $x = 0.03$, (d) $x = 0.035$, (e) $x = 0.04$ and (f) $x = 0.05$.

all the ceramics throughout the studied composition range possess a high T_C of above 300°C, which is generally positive for practical application.

Figure 7 plots the room-temperature d_{33} and k_p of the poled KNN-*x*BLZ-CZ ceramics as functions of x. One can note that the ceramic $x = 0.035$ displays the optimal piezoelectric properties, with $d_{33} = 241$ pC/N and $k_p = 0.37$. It is the formed R–T phase boundary that contributes to the enhanced piezoelectric properties, just as it has done in many other KNN-based ceramics,[30,31] as the coexistence of multiple phases can facilitate the switching of domains during poling.[32,33] However, both the d_{33} and k_p drastically drop with further increasing BLZ content. This should mainly be ascribed to the structural evolution from the multiple phase coexistence to a single rhombohedral phase, and, additionally, the decreased sintering activity is, to a certain degree, responsible for the deterioration of piezoelectric properties as well.

It has been widely accepted that not only excellent electrical properties but also a high T_C are crucial for the practical application of piezoelectric materials. For example, commercially available PZT ceramics usually possess both superior piezoelectric properties and a relatively high T_C ($\sim$ 300°C), as listed in Table I. By contrast, the piezoelectric properties of pure KNN are too poor for practical

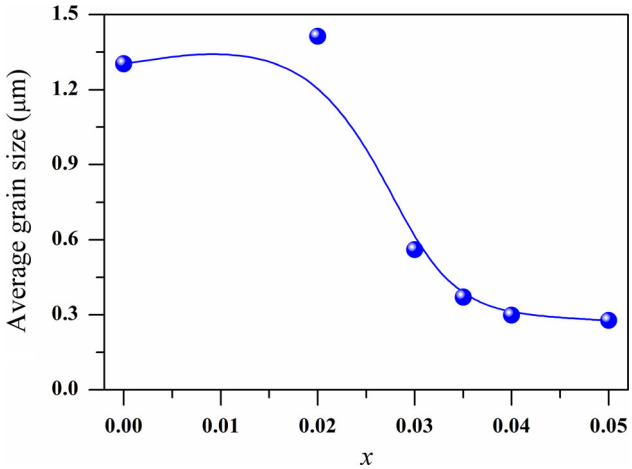

Fig. 4. Average grain size of KNN-*x*BLZ-CZ ceramics as a function of *x*.

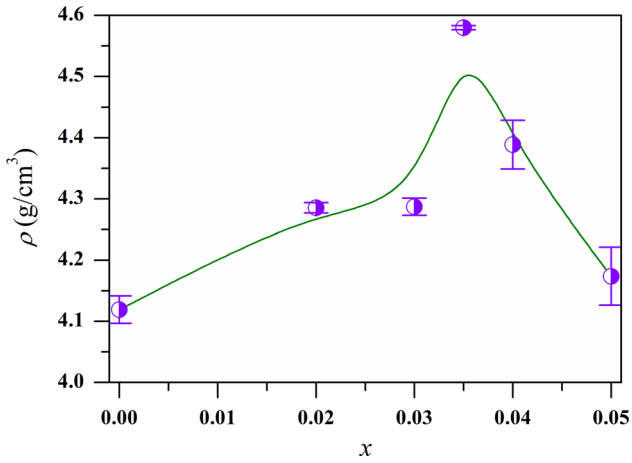

Fig. 5. Density of the KNN-*x*BLZ-CZ ceramics as a function of the BLZ content.

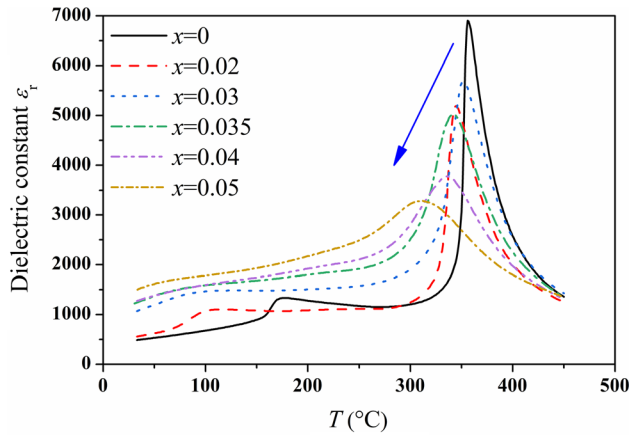

Fig. 6. Temperature-dependent dielectric constants of KNN-*x*BLZ-CZ ceramics, measured from room temperature to 450°C.

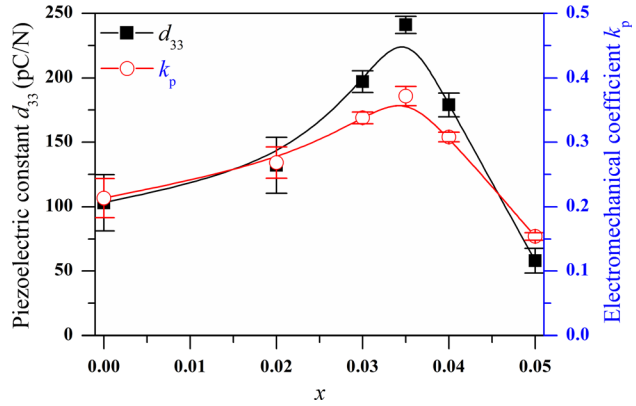

Fig. 7. Room-temperature d_{33} and k_p of KNN-*x*BLZ-CZ ceramics as functions of the BLZ content.

use. Although some doped KNN-based polycrystals have exhibited a piezoelectric activity almost comparable to that of commercial PZT materials, their T_C values are rather low. In comparison, the KNN-*x*BLZ-CZ ceramics researched in this work are characterized by both relatively good piezoelectric properties and a high T_C.

The *P*–*E* hysteresis loops of the KNN-*x*BLZ-CZ ceramics with the compositions near the R–T phase boundary, which were measured at room temperature and 10 Hz, have been plotted in Fig. 8 to evaluate their ferroelectric performance. One can see that although the ferroelectricity of the ceramic system shows an obvious dependence on BLZ content, all hysteresis loops have a substantially saturated shape, which confirms the previous inference that the compositions x = 0.04–0.5 possess a ferroelectric rhombohedral structure rather than a paraelectric cubic structure. Furthermore, the remnant polarization (P_r) exhibits a decreasing trend within the studied composition range with the increase in BLZ content, and this is consistent with the impact of other BMZ-type compounds on the ferroelectricity of KNN.[16,29]

CONCLUSION

In this work, phase-pure perovskite KNN-*x*BLZ-CZ ceramics can be obtained by a conventional solid-state sintering method. The increasing BLZ addition contents shift both the T_{R-O} and T_{O-T} of the ceramics towards room temperature, and accordingly induce a gradual structural evolution from an orthorhombic to a rhombohedral symmetry. An R–T phase boundary is formed at x = 0.035, near which the ceramics exhibit the optimum piezoelectric properties, with piezoelectric constant d_{33} = 241 pC/N and planar electromechanical coupling coefficient k_p = 0.37. The incorporation of BLZ into KNN-based ceramics will hinder the growth of grains during sintering, due to the aggregation of Bi^{3+} and Zr^{4+} ions at grain boundaries. A diffuse phase transition is caused by adding the BLZ to a

Table I. Comparison of piezoelectric properties between KNN-based ceramics and commercially available PZT ceramics

Materials	d_{33} (pC/N)	k_p	T_C (°C)	References
PZT4	410	0.60	250	Saito[34]
PZT5A	374	0.60	365	Shi[35]
PZT (MT-18 K)	340	0.60	300	Matsuoka[36]
$K_{0.475}Na_{0.525}NbO_3$	106	0.35	425	Yin[37]
KNN-BNZ-AS-Fe	500	0.50	< 200	Zheng[38]
KNN-BLZ-CZ	241	0.37	342	This work

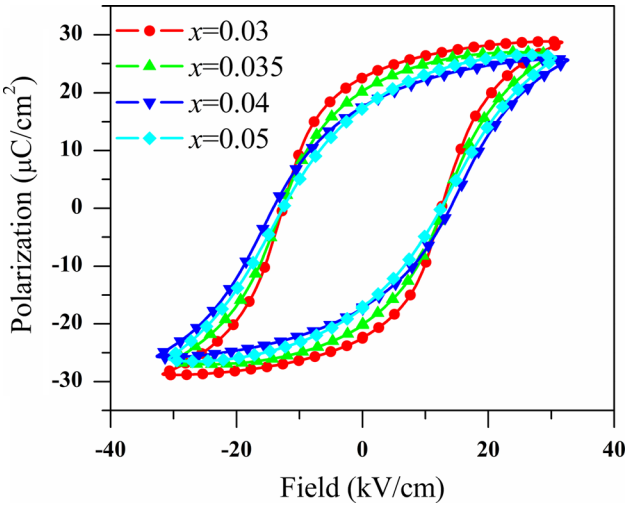

Fig. 8. Room-temperature *P–E* hysteresis loops of KNN-*x*BLZ-CZ ceramics with different BLZ contents, measured at 10 Hz.

relatively high amount. Moreover, it is found that although increasing BLZ content leads to a reduction in the T_C of the ceramics, the T_C can still maintain a high value of above 300°C in the studied composition range $0 \le x \le 0.05$. To sum up, our results can provide a reference for the construction of a phase boundary and improvement of piezoelectric properties in (K,Na)NbO_3-based ceramics.

ACKNOWLEDGMENTS

This work was supported by the Fundamental Research Funds for the Central Universities (nos. XDJK2020B003 and SWU117018) and the Research Project of Chongqing Municipal Education Commission (no. yjg183037).

REFERENCES

1. J. Wu, D. Xiao, and J. Zhu, *Chem. Rev.* 115, 2559 (2015).
2. P.K. Panda and B. Sahoo, *Ferroelectrics* 474, 128 (2015).
3. Y. Liu, Y. Yi, Y. Yu, Y. Pan, C. He, X. Liu, Z. Xu, G. Liu, and Y. Chen, *Ceram. Int.* 45, 6328 (2019).
4. S. Zhang, R. Xia, and T.R. Shrout, *J. Electroceram.* 19, 251 (2007).
5. Y. Liu, Y. Ding, X. Du, M. Shi, C. He, J. Li, X. Dai, Z. Xu, and Y. Chen, *J. Mater. Sci. Mater. Electron* 30, 17856 (2019).
6. J. Wang and L. Luo, *J. Appl. Phys.* 123, 144102 (2018).
7. Y. Yu, J. Li, X. Dai, Y. Yi, Y. Pan, C. He, Y. Liu, X. Liu, and Y. Chen, *Mater. Res. Express* 6, 106322 (2019).
8. J. Wu, H. Tao, Y. Yuan, X. Lv, X. Wang, and X. Lou, *RSC Adv.* 5, 14575 (2015).
9. Z. Cen, W. Feng, P. Zhao, L. Chen, C. Zhu, Y. Yu, L. Li, and X. Wang, *J. Am. Ceram. Soc.* 102, 2675 (2019).
10. T. Zheng, H. Wu, Y. Yuan, X. Lv, Q. Li, T. Men, C. Zhao, D. Xiao, J. Wu, K. Wang, J. Li, Y. Gu, J. Zhu, and S.J. Pennycook, *Energy Environ. Sci.* 10, 528 (2017).
11. B. Wu, H. Wu, J. Wu, D. Xiao, J. Zhu, and S.J. Pennycook, *J. Am. Chem. Soc.* 138, 15459 (2016).
12. K. Xu, J. Li, X. Lv, J. Wu, X. Zhang, D. Xiao, and J. Zhu, *Adv. Mater.* 28, 8519 (2016).
13. B. Wu, J. Ma, W. Wu, M. Chen, and Y. Ding, *Ceram. Int.* 44, 1172 (2018).
14. T. Zheng, J. Wu, D. Xiao, and J. Zhu, *Prog. Mater. Sci.* 98, 552 (2018).
15. Y. Pan, Y. Yu, Y. Yi, Y. Liu, J. Li, X. Dai, C. He, X. Liu, and Y. Chen, *Phys. B* 558, 122 (2019).
16. B. Kim, S. Yang, M. Lee, and G. Lee, *Ceram. Int.* 43, 15880 (2017).
17. Z. Cen, Y. Huan, W. Feng, Y. Yu, P. Zhao, L. Chen, C. Zhu, L. Li, and X. Wang, *J. Mater. Chem. A* 6, 19967 (2018).
18. N. Klein, E. Hollenstein, D. Damjanovic, H.J. Trodahl, N. Setter, and M. Kuball, *J. Appl. Phys.* 102, 014112 (2007).
19. Z. Fu, J. Yang, P. Lu, L. Zhang, H. Yao, F. Xu, and Y. Li, *Ceram. Int.* 43, 12893 (2017).
20. B. Malic, J. Koruza, J. Hrescak, J. Bernard, K. Wang, J.G. Fisher, and A. Bencan, *Materials* 8, 8117 (2015).
21. T. Shao, H. Du, H. Ma, S. Qu, J. Wang, J. Wang, X. Wei, and Z. Xu, *J. Mater. Chem. A* 5, 554 (2017).
22. Y. Chen, Y. Liu, D. Xue, Z. Xu, G. Liu, X. Liu, Z. Chen, and X. Jiang, *J. Alloys Compd.* 735, 68 (2018).
23. H. Wang and J. Wu, *J. Alloys Compd.* 628, 329 (2015).
24. X. Pang, J. Qiu, K. Zhu, and J. Luo, *J. Mater. Sci.* 46, 2345 (2010).
25. X. Peng, B. Zhang, L. Zhu, L. Zhao, R. Ma, B. Liu, and X. Wang, *J. Adv. Ceram.* 7, 79 (2018).
26. H. Zhang, X. Li, X. Chen, H. Zhou, X. Li, X. Yan, G. Liu, and J. Sun, *J. Electron. Mater.* 48, 4017 (2019).
27. B. Zhang, X. Wang, X. Cheng, J. Zhu, D. Xiao, and J. Wu, *J. Alloys Compd.* 581, 446 (2013).
28. A. Munpakdee, K. Pengpat, J. Tontrakoon, and T. Tunkasiri, *Smart Mater. Struct.* 15, 1255 (2006).
29. T. Zheng, J. Wu, D. Xiao, J. Zhu, X. Wang, and X. Lou, *J. Mater. Chem. A* 3, 1868 (2015).
30. M. Lee, S. Yang, J. Park, and G. Lee, *Sci. Rep.* 9, 4195 (2019).
31. D. Xue, Y. Liu, M. Shi, P. Wang, L. Zhang, G. Liu, Z. Chen, and Y. Chen, *J. Mater. Sci. Mater. Electron* 29, 2072 (2018).
32. H. Tao, H. Wu, Y. Liu, Y. Zhang, J. Wu, F. Li, X. Lyu, C. Zhao, D. Xiao, J. Zhu, and S.J. Pennycook, *J. Am. Chem. Soc.* 141, 13987 (2019).
33. K. Zhang, Y. Guo, D. Pan, H. Duan, Y. Chen, H. Li, and H. Liu, *J. Alloys Compd.* 664, 503 (2016).

34. Y. Saito, H. Takao, T. Tani, T. Nonoyama, K. Takatori, T. Homma, T. Nagaya, and M. Nakamura, *Nature* 432, 84 (2004).
35. H. Shi, J. Chen, R. Wang, and S. Dong, *J. Alloys Compd.* 655, 290 (2016).
36. T. Matsuoka, H. Kozuka, K. Kitamura, H. Yamada, T. Kurahashi, M. Yamazaki, and K. Ohbayashi, *J. Appl. Phys.* 116, 154104 (2014).
37. J. Yin, J. Wu, and H. Wang, *J. Mater. Sci. Mater. Electron* 28, 4828 (2017).
38. T. Zheng, Y. Zhang, Q. Ke, H. Wu, L.W. Heng, D. Xiao, J. Zhu, S.J. Pennycook, K. Yao, and J. Wu, *Nano Energy* 70, 104559 (2020).